Ceramics International 48 (2022) 16010–16014

Contents lists available at ScienceDirect

Ceramics International

journal homepage: www.elsevier.com/locate/ceramint

A theoretical and experimental investigation on the SHS synthesis of (HfTiCN)-TiB_2 high-entropy composite

N.S. Evseev [a,*], A.E. Matveev [a], P.Yu. Nikitin [a], Yu.A. Abzaev [b], I.A. Zhukov [a]

[a] Tomsk State University, Russia
[b] Tomsk State University of Architecture and Building, Russia

ARTICLE INFO

Keywords:
High-entropy ceramics
HECs
Ab initio
USPEX
Borides

ABSTRACT

In this work, a fundamental possibility of obtaining a high-entropy ceramic (HfTiCN)-TiB_2 composite material by the coupled self-propagating high-temperature synthesis is shown. To search for a stable fixed composition of the HfTiCN compound, the USPEX code was used with the CASTEP interface at 0K. According to the XRD analysis, the obtained SHS product is represented by HfTiCN phase (60 wt%) and TiB_2 phase (40 wt%). Based on the results of XRD, elemental analysis, and the heat pattern of combustion of the Hf-Ti-C-N-B powder mixture, a probable mechanism for the formation of the (HfTiCN)-TiB_2 composite material during the coupled self-propagating high-temperature synthesis was proposed.

1. Introduction

The continuous development of materials science irreversibly entails the discovery of new materials and compounds. Along with this, the theoretical base is also developing. However, some seemingly fundamental and traditional paradigms cannot be applied to certain materials, in particular to high-entropy alloys (HEAs) [1] and high-entropy ceramics (HECs) [2]. As suggested, high-entropy materials are a mixture of 5 or more elements that form a single-phase compound (high-entropy materials have their own diffraction pattern), the Gibbs free energy of which is less than the Gibbs free energy of all possible existing compounds of these elements. An unexpected and extremely attractive feature of high-entropy materials is that their final properties are not equal to the average properties of the components, but often either exceed them, or are extraordinary and new. For example, (HfNbTaTiZr)C high-entropy ceramics have oxidation resistance at 800 °C compared to binary carbides, which have oxidation resistance only at 200 °C [3–5]. In general, high-entropy materials and, in particular, high-entropy ceramics can be used as functional and structural materials (Perovskite oxides [6,7], (HfMoTaTi)(BC)–SiC [8], (MoNbTaTiW)Si_2 [9]), materials for energy storage ((MgCoNiCuZn)O and derivatives [10,11]), thermoelectrics ((AgBiGe)Se [12], (Cu_5GeMgSnZn)S_9 [13]).

Despite the successful application in many works of thermodynamic calculations to assess the existence of high-entropy (and any other) compounds, they may not always be truly correct. A striking example of this statement is the study of aluminum-magnesium boride $AlMgB_{14}$ [14–17]. Despite the unconditionally stable and repeatedly proven existence of this compound, thermodynamic calculations performed using the AFLOW utility [18] show its absence. In turn, another more promising approach is to predict the existence of thermodynamically stable compounds within the framework of Ab initio calculations using the USPEX code. Using this approach, a lot of new materials were discovered, in particular, superconducting materials based on lanthanum-yttrium ternary hydrides and others [19]. It should be noted that using classical packages for Ab initio calculations (VASP, CASTEP, QUANTUM ESPRESSO, etc.), the authors generate cubic supercells with given crystal lattice parameters. An important advantage of using USPEX as applied to high-entropy ceramics is that it generates all kinds of input files of the structure, not limited to cubic and hexagonal close-packed lattices, traditional for HECs [2], which opens up the possibility of searching for new non-standard compositions.

The search for high-entropy ceramics also includes the search for high-entropy composites. In Ref. [8], a high-entropy composite (HfMoTaTi)(BC)–SiC was obtained, the hardness of which was 35.4 GPa (by 48% higher than the theoretical value). It is important to note that the use of elements with high melting point (in particular, hafnium) as initial materials requires the use of spark plasma sintering [20–22] or hot pressing to obtain dense bulk samples. Moreover, there are compounds with a higher melting point. In 2015, as a result of theoretical studies (USA), it was found that a material based on hafnium, carbon

* Corresponding author.
E-mail address: evseevns@gmail.com (N.S. Evseev).

https://doi.org/10.1016/j.ceramint.2022.02.144
Received 18 December 2021; Received in revised form 25 January 2022; Accepted 14 February 2022
Available online 18 February 2022

Table 1
Purity and dispersion of the starting powders.

Powder	Purity, %	Dispersion, μm
Hafnium (Hf)	>99.0	<300.0
Titanium (Ti)	>99.0	<280.0
Boron (B)	>99.0	<0.6
Carbon (C)	>99.0	<0.8

and nitrogen (HfCN) can have a melting point of more than 4200 °C [23]. In 2019, a team of Russian scientists (MISiS) obtained a type of hafnium carbonitride with the chemical formula $HfC_{0.5}N_{0.35}$ [24].

As an alternative method for obtaining high-entropy composites, the method of self-propagating high-temperature synthesis (SHS) can be used. Today, SHS is an extremely effective method for the production nitrides, carbides, and borides [25–33]. In our previous works, we proposed two new methods for the production of aluminum-magnesium boride $AlMgB_{14}$. The first method is a thermochemical-coupled SHS of $AlMgB_{14}$–TiB_2 composite materials from a ($Al_{12}Mg_{17}$–B)-(Ti + 2B) powder mixture. The advantage of this method is that $AlMgB_{14}$ is formed due to the strongly exothermic reaction of titanium and boron (4250 kJ/kg, T_{ad} = 3193K), i.e. without the supply of additional heat from external sources. The second method is the so-called chemical furnace: ($Al_{12}Mg_{17}$–B) sample is placed in a highly exothermic mixture of titanium and silicon, the heat from which (as in the first method) is spent on the formation of $AlMgB_{14}$. In both cases, high-purity powder materials were obtained, which were then successfully consolidated by spark plasma sintering. Based on the foregoing, we assume that, due to the extremely high reaction temperatures, the SHS method can be successfully applied to obtain high-entropy ceramic composite materials from elements with a high melting point.

In this work, the elements of Hf, Ti, B, C and N were used as the initial components. Thus, the purpose of this work is to study the high-entropy ceramic composite of the Hf-Ti-C-N-B system obtained by self-propagating high-temperature synthesis.

2. Materials and methods

2.1. Raw components

Powders of hafnium, titanium, boron and carbon were used as initial materials. Dispersion and purity of the initial powders are presented in Table 1.

2.2. Experimental part

The initial components were mixed in the ratio (wt%): 32Ti + 8C + 26.7Hf + 3.3B. This composition was chosen for the following reasons. Titanium and carbon are mixed in a stoichiometric ratio at which titanium carbide is formed. Hafnium and boron were mixed in a stoichiometric ratio at which hafnium diboride is formed. The stoichiometric ratio of elements was taken to maximize the release of heat, which is sufficient for the implementation of coupled exothermic reactions. However, since the initial titanium powder was slightly finer than the hafnium powder, the TiC to HfB_2 ratio was increased in the initial mixture. The resulting powder mixture were cold-pressed into specimens with a diameter of 23 mm and a mass of 20 g. The pressure was 25 MPa. The obtained samples were placed in a constant pressure reactor, which was then evacuated. After evacuation, the reactor was filled with gaseous nitrogen to a pressure of 3.5 MPa for subsequent nitriding of the samples during SHS. Nitrogen of special purity (GOST 9293-74, 99.99%) was used in this work. The synthesis reaction was initiated by heating the upper surface of the sample with a molybdenum spiral.

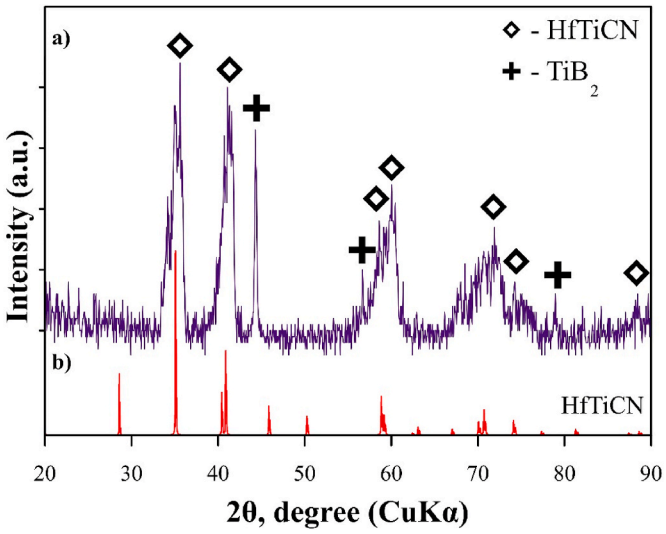

Fig. 1. a) Experimental XRD pattern of the combustion products of the Hf-Ti-C-N-B system, b) reference XRD pattern of the HfTiCN compound.

2.3. Characterization

To measure the combustion temperature, tungsten-rhenium thermocouple WR5/20 was introduced into the sample. The registration of the signal in the form of diffraction patterns on a computer was recorded by multichannel measuring-regulators "TPM-138" (OWEN) and an NL-8AI meter (from RealLab). Subsequent processing was performed using the "OWEN MANAGER ORM v.1" and "RealLab" programs. X-ray structural studies of the obtained synthesis products were performed on a Shimadzu 6000 diffractometer with CuKα-radiation. To determine the phase composition, the lattices of the PDF4+ crystallographic database and the predicted structures of the Hf-Ti-C-N system were used (the details of the calculations are given in the section "Computational details"). The microstructure of the obtained synthesis products was determined using a QUANTA 200 3D microscope equipped with an energy dispersive attachment (EDS).

2.4. Computational details

The prediction of the fixed composition of the HfTiCN compound was performed using the USPEX code [34–37] with the CASTEP [38] interface at 0K. The search for stable and quasi-stable configurations was carried out among compounds with different space groups (2–230). In CASTEP calculations, ultrasoft pseudopotentials were used with a plane-wave cutoff energy of 400 eV. All stable structures were optimized with force convergence during the relaxation to 10^{-6} eV/Å. In the USPEX calculations, the following parameters were chosen: the initial population size was 50, the total generation number was 35, the number of structures per generation was 45. FracGene (fraction of the generation produced by heredity), fracRand (fraction of the generation produced randomly from space groups), fracAtomsMut (fraction of the generation produced by sofmutation) was 0.5, 0.3 and 0.2, respectively. The predicted HfTiCN structure with the lowest energy was used for X-ray diffraction analysis and identification of the phase composition. The phase composition was refined using the Rietveld method. In this work, the CASTEP program code [38] was used to calculate the energies of the reference and refined crystal lattices within the framework of the density functional theory (DFT) using the generalized-gradient approximation (GGA).

3. Results and discussion

The XRD pattern of the obtained combustion products of the Hf-Ti-C-

Table 2
Structural parameters of the crystal lattices in the combustion products.

Phase	State	a, Å	c, Å	α = β	γ	V, Å^3	E, eV
HfTiCN	Reference	3.119	4.459	90.00	90.00	43.391	−2442.29
	Refined	3.071	4.357	90.00	90.00	41.105	−2441.87
TiB_2	Reference	3.029	3.228	90.00	120.00	25.655	−1760.71
	Refined	2.997	3.218	90.00	120.00	25.034	−1760.69

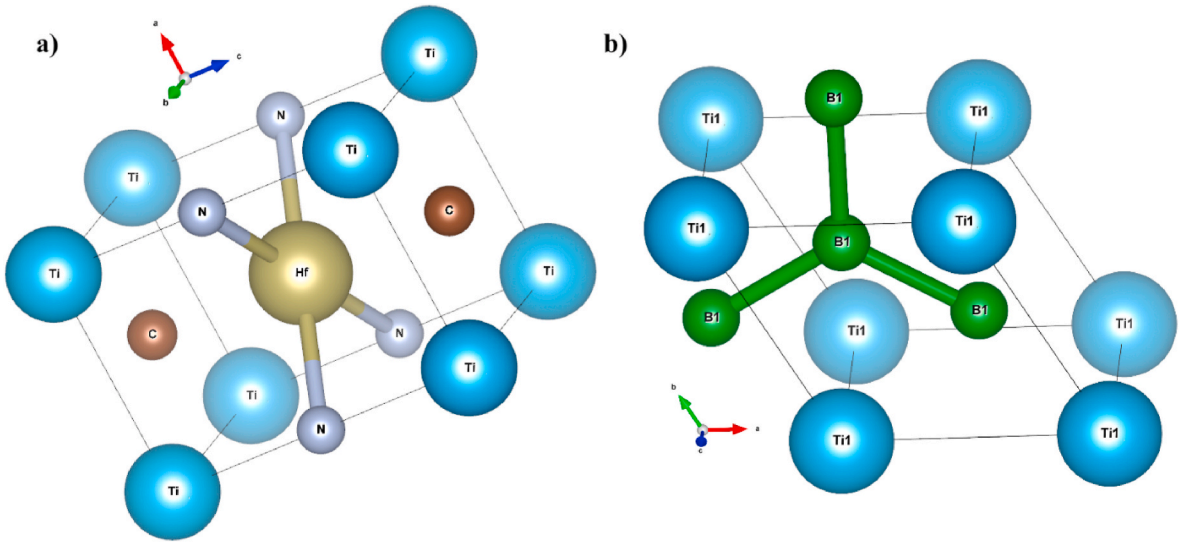

Fig. 2. 3D images of the HfTiCN (a) and TiB_2 (b) lattices.

N-B system is shown in Fig. 1. According to the XRD results, the TiB_2 and HfTiCN phases were found in the combustion products. It was found that the predicted HfTiCN compound (Fig. 1b) approximates well the experimental XRD pattern of the obtained material (Fig. 1a).

Table 2 shows the reference and refined parameters of the HfTiCN and TiB_2 phases (structural parameters, volume and lattice energy). The reference and refined lattices are slightly different. The HfTiCN crystal lattice has a P4/MMM space group, while the TiB_2 crystal lattice has a P6/MMM space group.

According to the Rietveld method, the HfTiCN phase content in the obtained SHS products is approximately 60 wt%, and the TiB_2 phase content is approximately 40 wt%. Fig. 2 shows 3D images of the HfTiCN and TiB_2 lattices after the refinement of the structural parameters by the Rietveld method.

SEM images of the microstructure of the combustion products are shown in Fig. 3a and b. It was found that the structure of the SHS products is represented by dark and light particles. EDS analysis showed that the elements of boron and titanium dominate in the dark areas, which corresponds to the TiB_2 phase. The elements of Hf, C, N, and Ti were found in the bright areas, which corresponds to the HfTiCN phase. The elemental analysis results are in good agreement with the results of X-ray structural analysis. Based on the obtained data, it was found that during SHS synthesis, boron particles react with titanium particles and form the TiB_2 phase. In this case, a clear interface is formed between the TiB_2 and HfTiCN particles. This is confirmed by the mapping results (Fig. 3c–h).

Fig. 4 shows a heat pattern obtained during the coupled self-propagating high-temperature synthesis of the Hf-Ti-C-N-B composite mixture. Based on the obtained heat pattern, XRD results and elemental analysis, a probable mechanism for the formation of the (HfTiCN)-TiB_2 composite material was proposed.

The heating of the spiral initiates an exothermic reaction in the upper layer of the sample. Heat from this reaction is transferred to the main part of the sample by conductive and convective transfer. Under the influence of heat, titanium particles melt, followed by saturation with boron and carbon particles. Since the enthalpy of formation of titanium diboride (−321.5 kJ/mol) [39] is lower than the enthalpy of formation of titanium carbide (−133.7 kJ/mol) [40], after saturation of the titanium melt with boron and carbon, an exothermic reaction of the TiB_2 formation occurs. During the exothermic reaction, a large amount of heat is released, characterized by a sharp increase in temperature to 2250 °C (a peak 1 on the heat pattern). The heat released during the exothermic reaction is consumed to melt the hafnium particles and dissolve the remaining carbon particles in the resulting melt. Moreover, the obtained melt is saturated with gaseous nitrogen, after which an exothermic reaction of the HfTiCN formation occurs with the release of heat, characterized by an increase in temperature to 2100 °C (peaks 2–3 on the heat pattern). A peak 4 characterizes the completion of the synthesis processes and the cooling of the obtained SHS products. After cooling, a composite structure is formed in the synthesis products, consisting of titanium diboride particles distributed between HfTiCN particles.

4. Conclusion

In this work, the fundamental possibility of obtaining the high-entropy ceramic (HfTiCN)-TiB_2 composite by self-propagating high-temperature synthesis is shown. Ab initio calculations showed the existence of the stable high-entropy HfTiCN compound with the P4/MMM space group. According to the results of X-ray diffraction analysis, the content of the HfTiCN and TiB_2 phases in the obtained composite is approximately 60 and 40 wt%, respectively. According to the obtained SEM images and the results of elemental analysis, the microstructure of the composite is represented by two phases: TiB_2 and HfTiCN, which have a clear interface between each other. Based on the obtained results, a probable mechanism for the formation of the (HfTiCN)-TiB_2 composite was proposed.

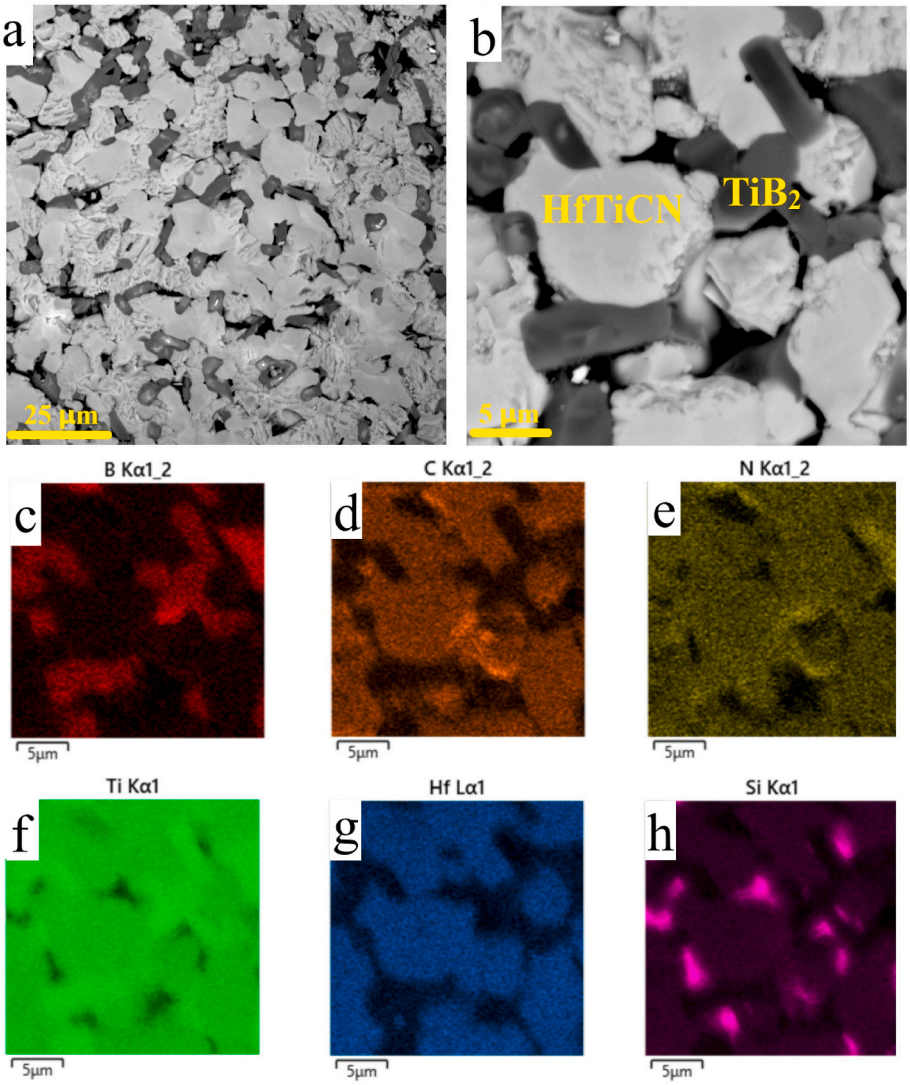

Fig. 3. SEM images of the microstructure (a–b) and mapping (c–h) of obtained SHS products.

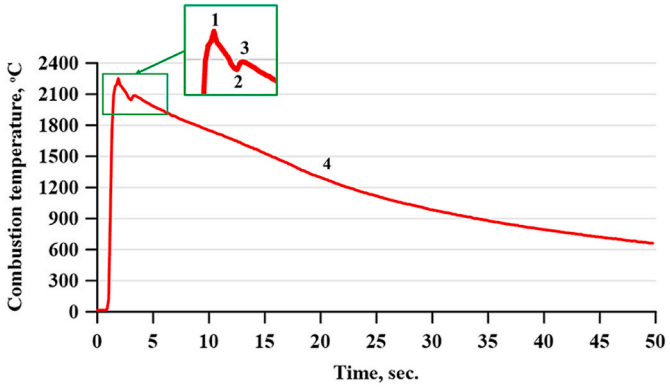

Fig. 4. Heat pattern obtained during the combustion of the Hf-Ti-C-N-B systems.

Credit author statement

Nikolay Evseev: Conceptualization, Methodology, Visualization, Writing – Original Draft; **Alexey Matveev:** Methodology, Investigation, Writing – Review and Editing; **Pavel Nikitin:** Methodology, Investigation, Modeling; Writing – Review and Editing, Translating; **Yuriy Abzaev:** Investigation, Modeling; **Ilya Zhukov:** Supervision, Resources.

Funding

This work was carried out with financial support of the grant from the President of the Russian Federation MK-3236.2021.4.

Declaration of competing interest

The authors declare that they have no known competing financial interests or personal relationships that could have appeared to influence the work reported in this paper.

References

[1] E.P. George, D. Raabe, R.O. Ritchie, High-entropy alloys, Nat. Rev. Mater. 4 (8) (2019) 515–534, https://doi.org/10.1038/s41578-019-0121-4.
[2] C. Oses, C. Toher, S. Curtarolo, High-entropy ceramics, Nat. Rev. Mater. 5 (4) (2020) 295–309, https://doi.org/10.1038/s41578-019-0170-8.
[3] J. Zhou, J. Zhang, F. Zhang, B. Niu, L. Lei, W. Wang, High-entropy carbide: a novel class of multicomponent ceramics, Ceram. Int. 44 (17) (2018) 22014–22018, https://doi.org/10.1016/j.ceramint.2018.08.100.
[4] T.J. Harrington, J. Gild, P. Sarker, C. Toher, C.M. Rost, O.F. Dippo, C. McElfresh, K. Kaufmann, E. Marin, L. Borowski, P.E. Hopkins, J. Luo, S. Curtarolo, D.

W. Brenner, K.S. Vecchio, Phase stability and mechanical properties of novel high entropy transition metal carbides, Acta Mater. 166 (2019) 271–280, https://doi.org/10.1016/j.actamat.2018.12.054.
[5] B. Ye, T. Wen, K. Huang, C.-Z. Wang, Y. Chu, First-principles study, fabrication, and characterization of $(Hf_{0.2}Zr_{0.2}Ta_{0.2}Nb_{0.2}Ti_{0.2})C$ high-entropy ceramic, J. Am. Ceram. Soc. 102 (2019) 4344–4352, https://doi.org/10.1111/jace.16295.
[6] A. Sarkar, R. Djenadic, D. Wang, C. Hein, R. Kautenburger, O. Clemens, H. Hahn, Rare earth and transition metal based entropy stabilised perovskite type oxides, J. Eur. Ceram. Soc. 38 (5) (2018) 2318–2327, https://doi.org/10.1016/j.jeurceramsoc.2017.12.058.
[7] S. Jiang, T. Hu, J. Gild, N. Zhou, J. Nie, M. Qin, T. Harrington, K. Vecchio, J. Luo, A new class of high-entropy perovskite oxides, Scripta Mater. 142 (2018) 116–120, https://doi.org/10.1016/j.scriptamat.2017.08.040.
[8] H. Zhang, D. Hedman, P. Feng, G. Han, F. Akhtar, A high-entropy B4(HfMo2TaTi)C and SiC ceramic composite, Dalton Trans. 48 (2019) 5161–5167, https://doi.org/10.1039/C8DT04555K.
[9] J. Gild, J. Braun, K. Kaufmann, E. Marin, T. Harrington, P. Hopkins, K. Vecchio, J. Luo, A high-entropy silicide: (Mo0.2Nb0.2Ta0.2Ti0.2W0.2)Si2, J. Materiomics. 5 (3) (2019) 337–343, https://doi.org/10.1016/j.jmat.2019.03.002.
[10] Q. Wang, et al., Multi-anionic and -cationic compounds: new high entropy materials for advanced Li-ion batteries, Energy Environ. Sci. 12 (2019) 2433–2442, https://doi.org/10.1039/C9EE00368A.
[11] D. Bérardan, S. Franger, D. Dragoe, A.K. Meena, N. Dragoe, Colossal dielectric constant in high entropy oxides, Phys. Status Solidi Rapid Res. Lett. 10 (2016) 328–333, https://doi.org/10.1002/pssr.201600043.
[12] S. Roychowdhury, T. Ghosh, R. Arora, U.V. Waghmare, K. Biswas, Stabilizing n-type cubic GeSe by entropydriven alloying of AgBiSe2: ultralow thermal conductivity and promising thermoelectric performance, Angew. Chem. Int. Ed. 57 (2018) 15167–15171, https://doi.org/10.1002/anie.201809841.
[13] R.-Z. Zhang, F. Gucci, H. Zhu, K. Chen, M.J. Reece, Data-driven design of ecofriendly thermoelectric high-entropy sulfides, Inorg. Chem. 57 (2018) 13027–13033, https://doi.org/10.1021/acs.inorgchem.8b02379.
[14] V.I. Matkovich, J. Economy, Structure of $MgAlB_{14}$ and a brief critique of structural relationships in higher borides, Acta Crystallogr. B 26 (5) (1970) 616–621, https://doi.org/10.1107/S0567740870002868.
[15] I.A. Zhukov, P.Y. Nikitin, A.B. Vorozhtsov, S.N. Perevislov, S.D. Sokolov, M. H. Ziatdinov, The use of intermetallic Al_xMg_y powder to obtain $AlMgB_{14}$-based materials, Mater. Today Commun. 22 (2020) 100848, https://doi.org/10.1016/j.mtcomm.2019.100848.
[16] P.Y. Nikitin, I.A. Zhukov, M.S. Boldin, S.N. Perevislov, V.N. Chuvil'deev, Spark plasma sintering, phase composition, and properties of $AlMgB_{14}$ ceramic materials, Russ. J. Inorg. Chem. 66 (8) (2021) 1252–1256, https://doi.org/10.1134/S0036023621080167.
[17] P.Y. Nikitin, I.A. Zhukov, A.B. Vorozhtsov, Decomposition mechanism of $AlMgB_{14}$ during the spark plasma sintering, J. Mater. Res. Technol. 11 (2020) 687–692, https://doi.org/10.1016/j.jmrt.2021.01.044.
[18] C. Oses, E. Gossett, D. Hicks, F. Rose, M.J. Mehl, E. Perim, I. Takeuchi, S. Sanvito, M. Scheffler, Y. Lederer, O. Levy, C. Toher, S. Curtarolo, AFLOW-CHULL: cloud-oriented platform for autonomous phase stability analysis, J. Chem. Inf. Model. 58 (12) (2018) 2477–2490, https://doi.org/10.1021/acs.jcim.8b00393.
[19] D.V. Semenok, I.A. Troyan, A.G. Ivanova, A.G. Kvashnin, I.A. Kruglov, M. Hanfland, A.V. Sadakov, O.A. Sobolevskiy, K.S. Pervakov, I.S. Lyubutin, K. V. Glazyrin, N. Giordano, D.N. Karimov, A.L. Vasiliev, R. Akashi, V.M. Pudalov, A. R. Oganov, Superconductivity at 253 K in lanthanum–yttrium ternary hydrides, Mater. Today 48 (2021) 18–28, https://doi.org/10.1016/j.mattod.2021.03.025.
[20] A.S. Mukasyan, A.S. Rogachev, D.O. Moskovskikh, ZhS. Yermekova, Reactive spark plasma sintering of exothermic systems: a critical review, Ceram. Int. (2021), https://doi.org/10.1016/j.ceramint.2021.10.207.
[21] L. Ma, Z. Zhang, B. Meng, M. Wan, Effect of pressure and temperature on densification in electric field-assisted sintering of inconel 718 superalloy, Materials 14 (10) (2021) 2546, https://doi.org/10.3390/ma14102546.
[22] S. Vorotilo, A.A. Nepapushev, D.O. Moskovskikh, V.S. Buinevich, G.V. Trusov, D. Yu Kovalev, A.O. Semenyuk, N.D. Stepanov, K. Vorotilo, A.Y. Nalivaiko, A. A. Gromov, Engineering of strong and hard in-situ Al-Al3Ti nanocomposite via high-energy ball milling and spark plasma sintering, J. Alloys Compd. (2021) 162676, https://doi.org/10.1016/j.jallcom.2021.162676.
[23] V.S. Buinevich, A.A. Nepapushev, D.O. Moskovskikh, G.V. Trusov, K.V. Kuskov, A. S. Mukasyan, Mechanochemical synthesis and spark plasma sintering of hafnium carbonitride ceramics, Adv. Powder Technol. 32 (2) (2021) 385–389, https://doi.org/10.1016/j.apt.2020.12.018.
[24] V.S. Buinevich, A.A. Nepapushev, D.O. Moskovskikh, G.V. Trusov, K.V. Kuskov, S. G. Vadchenko, A.S. Rogachev, A.S. Mukasyan, Fabrication of ultra-high-temperature nonstoichiometric hafnium carbonitride via combustion synthesis and spark plasma sintering, Ceram. Int. 46 (10, Part B) (2020) 16068–16073, https://doi.org/10.1016/j.ceramint.2020.03.158.
[25] Y.V. Bogatov, V.A. Shcherbakov, O.D. Boyarchenko, Preparation of dense TiB_2 by forced self-propagating high-temperature synthesis compaction with mechanical activation of reagents, Inorg. Mater. 57 (2021) 1061–1066, https://doi.org/10.1134/S0020168521100010.
[26] S. Aydinyan, S. Kharatyan, I. Hussainova, SHS-derived powders by reactions' coupling as primary products for subsequent consolidation, Materials 14 (17) (2021) 5117, https://doi.org/10.3390/ma14175117.
[27] V. Sanin, D. Andreev, D. Ikornikov, V. Yukhvid, Cast intermetallic alloys and composites based on them by combined centrifugal casting—SHS process, Open J. Met. 3 (2013) 12–24, https://doi.org/10.4236/ojmetal.2013.32A2003.
[28] P.Y. Nikitin, I.A. Zhukov, A.E. Matveev, S.D. Sokolov, M.S. Boldin, A. B. Vorozhtsov, $AlMgB_{14}$–TiB_2 composite materials obtained by self-propagating high-temperature synthesis and spark plasma sintering, Ceram. Int. 46 (14) (2020) 22733–22737, https://doi.org/10.1016/j.ceramint.2020.06.039.
[29] P.Y. Nikitin, A.E. Matveev, I.A. Zhukov, Energy-effective AlMgB14 production by self-propagating high-temperature synthesis (SHS) using the chemical furnace as a source of heat energy, Ceram. Int. 47 (15) (2021) 21698–21704, https://doi.org/10.1016/j.ceramint.2021.04.183.
[30] A. Matveev, I. Zhukov, M. Ziatdinov, A. Zhukov, Planetary milling and self-propagating high-temperature synthesis of Al-TiB_2 composites, Materials 13 (5) (2020) 1050, https://doi.org/10.3390/ma13051050.
[31] A. Matveev, P. Nikitin, I. Zhukov, A.S. Zhukov, The use of plastic waste as carbon raw materials to obtain TiC-based powders, Ceram. Int. 47 (1) (2021), https://doi.org/10.1016/j.ceramint.2021.04.117.
[32] N. Evseev, P. Nikitin, M. Ziatdinov, I. Zhukov, A. Vakutin, AlN production in Co-flow filtration mode at low pressures, Materials 14 (2021) 5482, https://doi.org/10.3390/ma14195482.
[33] N. Evseev, M. Ziatdinov, V. Romandin, A. Zhukov, A. Tolynbekov, Yu Ryzhikh, Process of obtaining chromium nitride in the combustion mode under conditions of Co-flow filtration, Processes 8 (9) (2020) 1056, https://doi.org/10.3390/pr8091056.
[34] A.R. Oganov, A.O. Lyakhov, M. Valle, How evolutionary crystal structure prediction works and why, Accounts Chem. Res. 44 (3) (2011) 227–237, https://doi.org/10.1021/ar1001318.
[35] A.O. Lyakhov, A.R. Oganov, H.T. Stokes, Q. Zhu, New developments in evolutionary structure prediction algorithm USPEX, Comput. Phys. Commun. 184 (4) (2013) 1172–1182, https://doi.org/10.1016/j.cpc.2012.12.009.
[36] A.R. Oganov, C.W. Glass, Crystal structure prediction using ab initio evolutionary techniques: principles and applications, J. Chem. Phys. 124 (24) (2006) 244704, https://doi.org/10.1063/1.2210932.
[37] N. Miao, J. Wang, Y. Gong, J. Wu, H. Niu, S. Wang, H. Hosono, Computational prediction of boron-based MAX phases and MXene derivatives, Chem. Mater. 32 (16) (2020) 6947–6957, https://doi.org/10.1021/acs.chemmater.0c02139.
[38] S.J. Clark, M.D. Segall, C.J. Pickard, P.J. Hasnip, M.I. Probert, K. Refson, M. C. Payne, First principles methods using CASTEP, Z. für Kristallogr. - Cryst. Mater. 220 (5–6) (2005) 567–570, https://doi.org/10.1524/zkri.220.5.567.65075.
[39] V.V. Akhachinskij, N.A. Chirin, Enthalpy of formation of titanium diboride, Thermodynamics of nuclear materials, in: International Atomic Energy Agency, Vienna (Austria); Proceedings Series; 2 v.; V. 2 P. 467- 476, IAEA; Vienna; Symposium on the thermodynamics of nuclear materials, Vienna, Austria, 1975, 21 Oct 1974.
[40] D.L. Vrel, J.M. Lihrmann, J.P. Petitet, Synthesis of titanium carbide by self-propagating powder reactions. 1. Enthalpy of formation of TiC, J. Chem. Eng. Data 40 (1) (1995) 280–282, https://doi.org/10.1021/je00017a062.